12-15-2007

Microstructural Investigations of the Layered Cathode Materials LiCoO2 and LiNi1/3Mn1/3Co1/3O2

Tanghong Yi
University of New Orleans

Microstructural Investigations of the Layered Cathode Materials $LiCoO_2$ and $LiNi_{1/3}Mn_{1/3}Co_{1/3}O_2$

A Thesis

Submitted to the Graduate Faculty of the
University of New Orleans
in partial fulfillment of the
requirements for the degree of

Master of Science
in
Chemistry

by

Tanghong Yi

B.S. University of Science and Technology of China, 2005

December 2007

ACKNOWLEDGEMENTS

First of all, I would like to express my sincere gratitude to my advisor, Professor Heike Gabrisch. Heike's enthusiasm and insights were constant inspirations during my course of study. I am also very grateful for her friendly, patient guidance and assistance and her support.

My gratitude also goes to the members of my committee, Professor Weilie Zhou, Professor John B. Wiley for their helpful comments and constructive suggestions.

I would like to give my special thanks to Professor Gerbrand Ceder in Massachusetts Institute of Technology, and Professor Marca M. Doeff in Lawrence Berkeley National Laboratory, who gave me generous help, let me study and work in their labs after the Hurricane Katrina.

I would like to acknowledge past and present group members, Qingfeng Xing, Mary Kombolias, Vaneet K. Sharma, James D. Wilcox, Juliette A.L. Saint, Guoying Chen, Xiaohua Ma, Fei Zhou, Ying Shirley Meng, Kisuk Kang, for their personal and professional exchanges, helps in my work, kindness and friendly environment.

Last, but not the least, great appreciation goes to my parents and elder sister for their love, encouragement and support throughout my life.

This work was supported by the Louisiana Board of Regents through contact number LEQSF (2004-07) –RD–A–36 and the Links Program (title: Investigation of the crystallographic and electronic structure of Li_xCoO_2 compounds).

TABLE OF CONTENTS

LIST OF FIGURES

LIST OF TABLES

ABSTRACT

Both $LiCoO_2$ and $LiNi_{1/3}Mn_{1/3}Co_{1/3}O_2$ layered cathode materials are investigated in our studies. P3 phase of CoO_2, the end member of the Li_xCoO_2, is found in both chemically and electrochemically delithiated materials. Delithiated Li_xCoO_2 specimens decompose into fine Co_3O_4 and $LiCoO_2$ particles starting at around 200 °C. This decomposing reaction is proved by in-situ X-ray diffraction and in-situ transmission electron microscopy investigations. The structures of pristine and cycled $LiNi_{1/3}Mn_{1/3}Co_{1/3}O_2$ are investigated by electron diffraction. Single and polycrystalline crystals are found in this material. The partial substitution of Co by Ni and Mn in $LiNi_{1/3}Mn_{1/3}Co_{1/3}O_2$ opens up the possibility of different cation configurations in the crystal lattice. Both $R\bar{3}m$ symmetry and superlattices are identified in this material. The number of particles with superlattices in pristine material (40%) is much bigger than cycled material at discharge state (10%).

Keywords: delithiation; phase transformation; LixCoO2; $LiNi_{1/3}Mn_{1/3}Co_{1/3}O_2$; X-ray diffraction; electron diffraction; superlattice.

INTRODUCTION

One of the hot topics and great challenges in the twenty-first century is unquestionably energy storage. People are trying to find the economic, efficiency and environmentally friendly energy conversion and storage systems responding to the needs of this world. Lithium ion batteries are one of the great successes of energy conversion and storage systems. Lithium ion batteries are the systems of choice, offering high energy density, flexible and lightweight design, and longer lifespan than comparable battery technologies. A historical account of the development of lithium ion batteries is about 30 years, counting from the first Li cell in 1970s. Nowadays, Lithium ion batteries play an important role in the portable devices, for example, cell phones, laptop computers, MP3 players like iPOD, and in larger application such as hybrid electric vehicles (HEV). Three main parts, anodes, electrolytes and cathodes make up the lithium ion batteries. The choice of the active material for the cathode determines the properties of the rechargeable battery. The structures that have received the most attention as possible positive electrode materials are spinel, α-$NaFeO_2$ –type layered, and orthorhombic structures. Layered structure cathode materials are attractive for researchers since they are easy for the movement of lithium ions during intercalation-deintercalation processes.

$LiCoO_2$ is the most common layered structure material used in commercial lithium ion batteries. The theoretical capacity of $LiCoO_2$ is 280 $mAhg^{-1}$, of which 140 $mAhg^{-1}$ is in general achieved due to the non-stability of $Li_{1-x}CoO_2$ ($0.5 < x < 1$). $LiCoO_2$ has good cycling performance and high upper cut-off voltage 4.2 V. On the other hand, the phase transitions of $LiCoO_2$ are complex, which have not been completely understood, especially, for low lithium

content $Li_{1-x}CoO_2$ in the range of $0.5 < x < 1$. In order to make those unsettled questions clear, we studied the lattice parameter changes and phase transitions with lithium contents in both chemically and electrochemically delithiated specimens $Li_{1-x}CoO_2$, and the phase transitions of delithiated $Li_{1-x}CoO_2$ as a function of temperatures. Both X-ray diffraction (XRD) and transmission electron microscopy (TEM) are employed to the phase characterization.

$LiNi_{1/3}Mn_{1/3}Co_{1/3}O_2$, is a new development based on $LiCoO_2$, with potential for applications in high power applications. Some of the disadvantages of $LiCoO_2$, e.g. environmental hazard and a high price are compensated in $LiNi_{1/3}Mn_{1/3}Co_{1/3}O_2$. $LiNi_{1/3}Mn_{1/3}Co_{1/3}O_2$ shows higher reversible capacity and thermal stability as well as lower cost than $LiCoO_2$. However, a low rate capability of the $LiNi_{1/3}Mn_{1/3}Co_{1/3}O_2$ has to be solved before commercialized in the lithium secondary battery. The structure of $LiNi_{1/3}Mn_{1/3}Co_{1/3}O_2$ is not as simple as $LiCoO_2$ with $R\bar{3}m$ symmetry. The distribution of three transition metals determines the structure of $LiNi_{1/3}Mn_{1/3}Co_{1/3}O_2$. The random Ni, Mn, and Co distribution in 3a positions in transition metal layer results in $R\bar{3}m$. The supercells are the common phenomena for $LiNi_{1/3}Mn_{1/3}Co_{1/3}O_2$. $[\sqrt{3}\times\sqrt{3}]R30^0$-type (space group $P3_112$) in triangular lattice of sites and pile-up model (space group P3m1) among CoO_2, NiO_2 and MnO_2 slabs are two superlattice models investigated using first principles calculations. In the second chapter of this thesis, we presented the experiments results of XRD and TEM characterizations of virgin $LiNi_{1/3}Mn_{1/3}Co_{1/3}O_2$ and specimens cycled in batteries.

CHAPTER 1

Investigation of Li_xCoO_2 Phases Produced by Heat Treatment of Delithiated $LiCoO_2$ Powders

1.1 Abstract:

$LiCoO_2$ is used as a cathode material in most commercial lithium-ion batteries. Of the phases formed upon Li-removal the P3 phase has been only reported in the chemically delithiated materials. In this paper we compare the microstructure of Li_xCoO_2 produced by chemical and electrochemical methods. P3 phase was found in both chemically (x = 0.59 for NO_2BF_4 oxidant) and electrochemically (x = 0.30) delithiated specimens. We investigate the phases formed in in-situ heating by X-ray diffraction and electron microscopy. Above approximate by 200°C Li_xCoO_2 decomposed into fine Co_3O_4 and $LiCoO_2$ particles.

Key words: delithiation; heat treatment; phase transformation; Li_xCoO_2; X-ray diffraction; Transmission electron microscopy

1.2 Introduction

Lithium ion batteries play an important role as power source in portable electronic devices. Currently $LiCoO_2$ is the most used active cathode material for commercial lithium ion batteries. It has been first suggested as intercalation compound for rechargeable Li-ion batteries by Mizushima et al..[1] Depending on synthesis temperature two crystallographic forms of $LiCoO_2$ are observed: at low temperatures around 350°C a cubic spinel structure is formed that converts

to a trigonal layered lattice around 900°C (space group 166, $R\bar{3}m$ also called hexagonal form). E. Rossen et al. compared the electrochemical performance of the cubic spinel form to that of the trigonal form and showed that the high temperature layered form has superior electrochemical properties.[2] The unit cell of the layered form consists of three slabs of edge sharing CoO_6 octahedra separated by interstitial layers of Li (O3 phase). With removal of Li from the layered crystal lattice during charge non stoichiometric Li_xCoO_2 compounds are formed that take on different crystallographic structures depending on Li-content. Structural consideration limit the amount of Li removed from the trigonal lattice to 0.5 which limits the achievable capacity to 140mA/g compared to the theoretical capacity of 270mAh/g. Many groups have studied the crystallographic changes that accompany variations in Li content. Reimers and Dahn carried out in-situ xrd experiments during charge of a coin cell and made the following observations: Upon Li-removal at a Li concentration of about Li = 0.93 a second hexagonal phase forms in addition to the original O3 phase. Between Li = 0.75 and Li = 0.93 the two hexagonal phases coexist while below Li = 0.75 only phase II is stable. Around a Li content of approximately 0.5 ordering of Li-vacancies leads to a monoclinic distortion of the lattice.[3] In a separate study by Ohzuku and Ueda found the same phases at slightly different Li-concentrations.[4] When all Li is removed from the lattice the edge sharing CoO_6 octahedra form a single layered unit cell called O1 phase that converts back to the original O3 phase with Li-reintercalation.[5] Theoretical and experimental studies have shown that more phases exist in the Li_xCoO_2 system: at low Li concentrations < 0.3 a mixture of O3 and O1 is observed (H1-3) phase that has been predicted by Van der Ven et al.[6] and experimentally observed by Chen et al..[7] Recently X.Q. Yang et al. reported new phases named by H2a as intermediate phase between H1 and H2 phases, and phase transitions during charge from 3.5V to 5.2V in coin cells.[8] According to X. Q. Yang's research

the phase diagram is made up by six single-phase regions (O3, H2a, M1, H1-3, M2, and O1) and two two-phase regions (O3 + H1-3 region for $0.78 < x < 0.9$ and H1-3 + M2 region for $0.15 < x < 0.25$). Studies by transmission electron diffraction revealed a phase transformation from the trigonal layered $LiCoO_2$ to a lithium depleted phase with the structure of a cubic spinel $Li_{2-x}Co_2O_4$ in samples of $LiCoO_2$ subjected to a high number of charge/discharge cycles indicating that the stable crystal structure depends on Li content.[9,10]

The volume of unit cell and lattice parameters of Li_xCoO_2 change with the lithium content. The c-lattice parameter increases up to a maximum around x equal to 0.5 followed by a decrease with further reduction in lithium content. The a-lattice parameter decreases slightly first and increases when x is less then 0.5. The changes of a-lattice parameter and c-lattice parameter oppose each other resulting in no big change of the volume of unit cell. This phenomenon was observed in both experiments[4] and simulations[6].

S. Venkatraman used chemical delithiation to study the crystal lattices formed with Li depletion. He showed that at high delithiation rates which are typical for chemical delithiation a metastable P3-type $CoO_{2-\delta}$ is formed that over time will transform into the stable O1 phase.[11]

Here we study the changes of unit cell dimensions and phases transformations with lithium removed from $LiCoO_2$. In order to identify the crystallographically stable phases corresponding to a composition Li_xCoO_2 we produce delithiated specimens and heat the powders to high temperatures. Characterization by x-ray diffraction indicates that P3 phase forms in both electrochemical and chemical delithiation. After heating the electrochemically delithiated powders to approximately 300°C for a short time (1 h) the P3 phase disappears and instead small amounts of Co_3O_4 are observed. In-situ electron microscopy and in-situ XRD indicate that $Li_{0.59}CoO_2$ starts to decompose to $LiCoO_2$ and Co_3O_4 at approximate 225°C.

1.3 Experimental details

$LiCoO_2$ used for coin cells and chemical delithiation was bought from Aldrich (purity>99.8%). The chemical delithiation was carried out using a solution of NO_2BF_4 in acetonitrile (CH_3CN). The delithiation reaction can be described by the equation $LiCoO_2 + x\ NO_2BF_4 \rightarrow Li_{1-x}CoO_2 + x\ NO_2 + x\ LiBF_4$. Different lithium contents x in Li_xCoO_2 are realized by adjusting the ratio of virgin $LiCoO_2$ to oxidant NO_2BF_4. 0.01 mole of $LiCoO_2$ and the proper amount of oxidant NO_2BF_4 were added into 20 mL CH_3CN solvent. Details are given in table 1.1. The solutions were stirred at room temperature for 3 hours.

The coin cells (CR2032) used for electrochemical delithiation were made of Li|1 M $LiPF_6$(EC:DMC = 1:1)|$LiCoO_2$ where EC and EMC stand for ethylene carbonate and dimethyl carbonate, respectively. The cathode mixtures contained 84 wt % active material $LiCoO_2$, 8 wt% SFG-6 synthetic flake graphite (Timcal, Ltd., Graphites and Technologies), and 8 wt % Kynar poly (vinylidene difluoride) (PVDF) binder, which was added as a 12 wt % solution (12 wt % Kynar and 88 wt % 1-methyl-2-pyrrolidone (NMP)). The paste was spread onto aluminum foil homogenously. The electrodes were dried overnight in air at ambient temperature and then in a vacuum oven at 120°C for 24 h. The electrodes were roll-pressed prior to use. The cells underwent 3 formation cycles between 3.0 and 4.2 V at the current corresponding to a charge rate of C/20 in galvanostatical channels of a Macpile II (Bio-Logic, SA, Claix, France). Then the cells were charged to different states at the current corresponding to a charge rate of 1C.[12] Table 1.2 gives a list of nominal compositions Li_xCoO_2 corresponding to the states of charge of each coin cell. The cells were disassembled immediately after the charging process, and washed with diethyl carbonate (DEC) to remove LiF from cathodes. For the electrochemically delithiated specimens the given Li concentration was calculated by the program Macpile.

Table 1.1: Chemically delithiated specimens using NO_2BF_4 as oxidant.

$LiCoO_2$: NO_2BF_4	ICP results
1 : 2	$Li_{0.59}CoO_2$
1 : 1	$Li_{0.87}CoO_2$
1 : 0.75	$Li_{0.83}CoO_2$

Table 1.2: Electrochemically delithiated specimens with coin cells.

	Charged voltage	Li_xCoO_2	Heating
Group 1	4.1 V	$Li_{0.79}CoO_2$	300 °C 1 h
	4.2 V	$Li_{0.64}CoO_2$	
	4.5 V	$Li_{0.49}CoO_2$	
	4.8 V	$Li_{0.30}CoO_2$	
Group 2	4.1 V	$Li_{0.69}CoO_2$	none
	4.5 V	$Li_{0.42}CoO_2$	
	4.8 V	$Li_{0.26}CoO_2$	

The electrochemical delithiated powders were aged in air for one hour at 300°C. Additionally in situ X-ray diffraction was applied to the chemically delithited specimen $Li_{0.59}CoO_2$ between 25°C and 325°C. This specimen $Li_{0.59}CoO_2$ was synthesized by Mary Kombolias with $K_2S_2O_8$ as oxidant.[13] The heating rate was 4 °C /min, and spectra were taken during relaxing periods.

X-ray diffraction (XRD) spectra were taken with a Philips X'-Pert diffractometer using Cu Kα radiation (λ = 1.54) to analyze phases. Silicon standard powder was used to ensure

accuracy in peak position determinations when it was necessary. Subsequently the materials were scraped off from the aluminum foil and washed with NMP and dried in a vacuum oven at ambient temperature. These powders were used for transmission electron microscopy (TEM) and ex-situ and in-situ heat treatment. Characterization by electron microscopy was carried out on a JEOL 3010 at Lawrence Berkeley National Laboratory.

The composition of chemically delithiated Li_xCoO_2 powders was measured by Inductively Coupled Plasma atomic emission spectroscopy (ICP-AES). Cobalt and lithium ICP/DCP standard solutions were bought from Sigma Aldrich. 100 mg of each the specimen Li_xCoO_2 was dissolved into 10 mL of high purity hydrocholoric acid (Alfa Aesar, 99.999999% metals basis) and then diluted to 250 mL before analysis in the ICP.

1.4 Results and discussion

1.4.1 Chemical and electrochemical delithiation

The XRD spectra of delithiated powders were compared in Figs. 1.1and 1.3. For both delithiation methods a small peak was observed to the right of the (003) peak of the O3 phase at low Li contents. The comparison of P3 and O1 XRD spectra was shown in Fig. 1.2. These two XRD spectra were simulated using PowderCell. Fig.1.1 showed the spectra of delithiated specimens from NO_2BF_4 oxidant. One obvious and also important difference of the XRD spectrum for $Li_{0.59}CoO_2$ comparing with others was the small peak close to (003) peak of O3 phase. This small peak was identified as (003) peak of P3 phase (CoO_2). P3 phase was also seen in $Li_{0.3}CoO_2$ produced by electrochemical delithiation, see Fig. 1.3. From the ratio of intensities, the amount of P3 phase was small compared to the amount of O3 phase.

Rietveld refinement of the experimental spectra considering a combination of O1 and O3 phase compared to a combination of P3 and O3 phase showed that this peak was best explained by presence of P3 phase. Furthermore, there are two easy way to exclude the possible phase of O1. First, the 2 theta of (001) peak of O1 phase is more than 20°, which does not match our observations. Secondly, the X-ray spectrum of O1 has two strong peaks (001) and (101) with almost equal intensity. However, there is no observation of additional small peak at the 2 theta position of (101) peak. The finding of a combination of O3 and P3 phase indicates that the extraction of lithium ions was not homogenous. Some parts of the particles or some particles lost all lithium ions to form CoO_2 (P3 phase), while the lithium content remained higher in other particles or areas of particles. Considering that lithium ions were removed from the surface of particles one could imagine that a gradient formed with a lower lithium content on the particle surface than in the core of particles. P3 phase should then be found predominantly on the surface of particles. We found P3 phase not only in chemically delithiated specimens but also in electrochemically delithiated Li_xCoO_2. As A. Manthiram reported, the metastable P3-type $CoO_{2-\delta}$ came from high delithiated rate by chemical delithiation.[11] That is why people only found out the stable O1 phase by electrochemical delithiation. However, the charge rate used in our study to fabricate delithiated specimens was very high with current corresponding to the charge rate of 1C. This should be the reason that we can achieve P3 phase in electrochemically delithiated specimens.

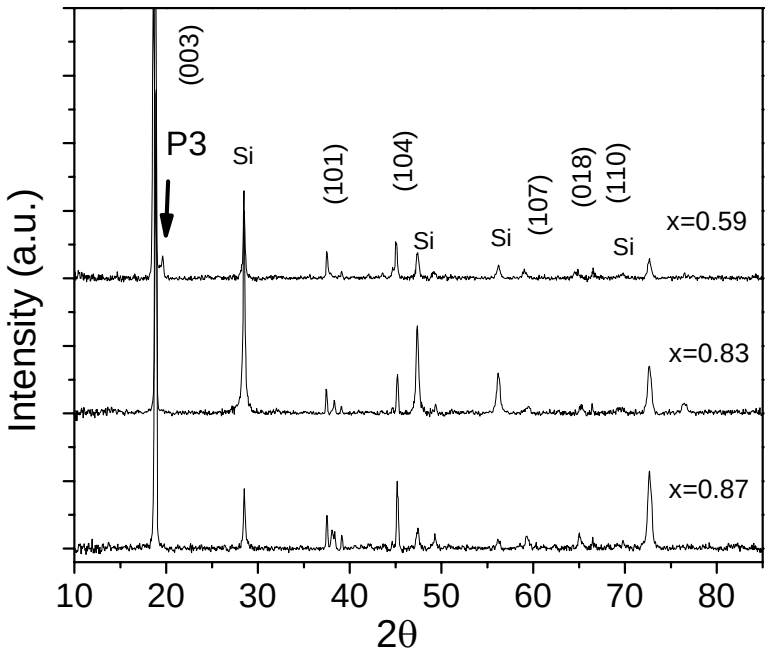

Fig.1.1: X-ray spectra of chemically delithiated specimens (x = 0.87, 0.83, 0.59).

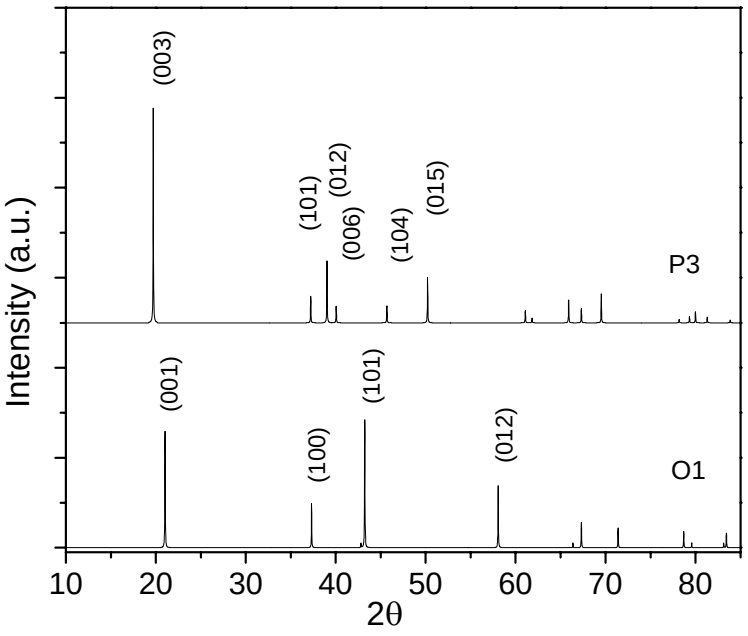

Fig.1.2: X-ray spectra of P3 and O1 phases from simulation.

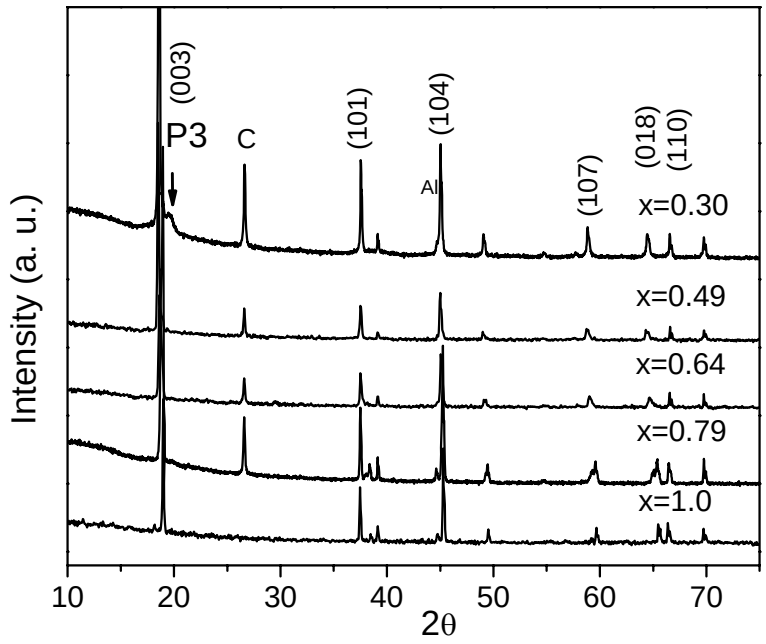

Fig.1.3: X-ray spectra of electrochemically delithiated products Li_xCoO_2 (x = 1.0, 0.79, 0.64, 0.49, 0.3).

Table 1.3 is showing the c-lattice parameters of a series of electrochemically delithiated specimens by coin cells from commercial $LiCoO_2$. Fig. 1.4 is the corresponding figure of c-lattice parameter changing as a function of lithium content x in Li_xCoO_2. The c-lattice parameter initially increased from 14.040 Å up to 14.373 Å when the lithium content decreased from 1 to 0.49. As lithium concentration was lowered further, the c-lattice parameter started to decrease after a maximum point.

Table 1.3: c-lattice parameters of electrochemically delithiated specimens.

Li_xCoO_2	(003)	c para./Å
X = 1.0	18.948	14.040
X = 0.79	18.936	14.048
X = 0.69	18.783	14.161
X = 0.64	18.603	14.297
X = 0.49	18.504	14.373
X = 0.42	18.511	14.367
X = 0.30	18.579	14.316
X = 0.26	18.664	14.251

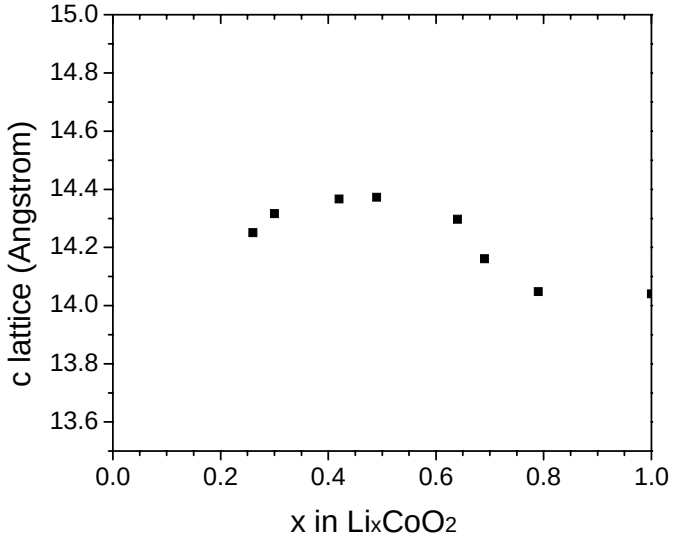

Fig.1.4: c-lattice parameter as a function of lithium content of electrochemically delithiated specimens.

1.4.2 Heat treatment

Heat treatment has been carried out to determine the stable structure for a given composition. By heating specimens we allowed them to attain their thermodynamic stable forms. The xrd spectra obtained from the electrochemically delithiated specimens after heating to 300°C are shown in Fig. 1.5. The delithiated products Li_xCoO_2 decompose to $LiCoO_2$ and Co_3O_4 after heat treatment, and the Li_xCoO_2 and P3 phases disappear. The intensity of peaks from Co_3O_4 (marked by an asterisk) is low compared to the intensity of the O3 peaks. However, the difference between the x-ray spectra of specimens before and after heat treatment is clear. The shoulders of (101) and (107) peaks of $LiCoO_2$ are the (311) and (511) peaks of Co_3O_4 (Fig. 1.5). Comparing the intensity ratio of (018) and (110) $LiCoO_2$ peaks in Fig. 1.3 to those in Fig. 1.5 we see that in Fig. 1.5 the (440) Co_3O_4 peak appears which overlaps with $LiCoO_2$ (018). The (220) peak of Co_3O_4 can be clearly seen in Fig. 1.5. Peak broadening is caused by the overlap of the (311), (511) and (440) peaks of Co_3O_4 with (101), (107) and (018) peaks of $LiCoO_2$ (Fig. 1.5). The similar results were found in chemically dethiated specimens with $K_2S_2O_8$ as oxidant by Kombolias.[13]

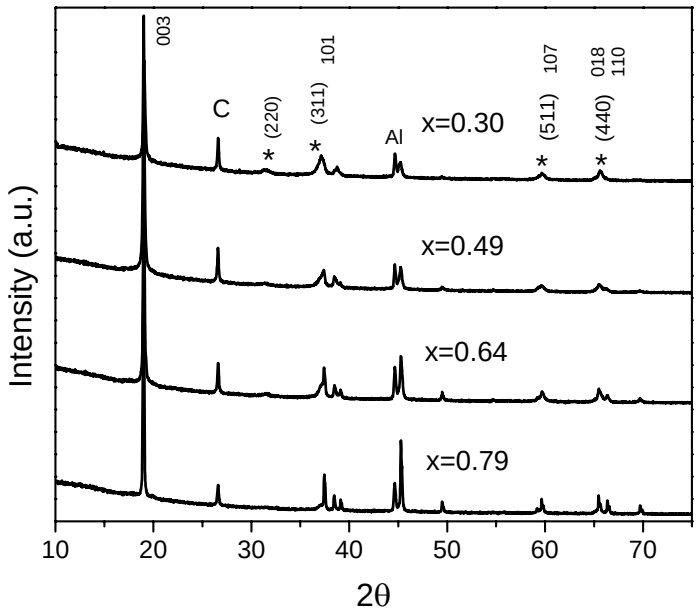

Fig.1.5: Electrochemically delithiated products Li_xCoO_2 (x = 1.0, 0.79, 0.64, 0.49, 0.3) after heat treatment at 300°C for 1 h.

In situ x-ray diffraction was carried out in the temperature range between 25°C and 325°C for the chemically delithiated sample $Li_{0.59}CoO_2$. In Fig. 1.6 the xrd scans taken during heating and cooling are shown in one diagram. Parts of the spectrum showing the (003) $LiCoO_2$ peak and the (220) Co_3O_4 peak are enlarged and shown to the left and right of the main spectrum respectively. Some of the features observed during heating and cooling are artifacts caused by changes in the instrument (thermal expansion of sample holder) during heating. These are a continuous shift of the whole spectrum to the left during heating and to the right during cooling. Additionally, the intensity of all peaks also went up and down with temperature.

Disregarding these artifacts two specimen related features were observed during heating:

- (220) and (311) peaks of Co_3O_4 appear in x-ray spectra starting at 225°C.
- The Li_xCoO_2 (003) peak shifts to a larger angle corresponding to a smaller lattice parameter at around 275°C.

The decomposition of Li_xCoO_2 into Co_3O_4 and $LiCoO_2$ starts before 225°C as indicated by the formation of a small (111) Co_3O_4 peak on the right side of the (003) peak of Li_xCoO_2 at 225°C. This temperature is believed to decrease with lithium content in Li_xCoO_2 since the stability of Li_xCoO_2 decreases with lithium content. The intensity of the newly formed Co_3O_4 peaks increases with temperature. Besides the contribution of the thermal expansion of the system, another reason is that the reaction of $Li_xCoO_2 \rightarrow LiCoO_2 + Co_3O_4$ continuous with heating time and temperature. This reaction is irreversible. Upon cooling to 25℃ the intensity of all peaks decreases due to the thermal expansion of the system. The enlarged section of the two theta range between 28-32° clearly shows that the thermal expansion of the system did us a favor by increasing the intensity of the weak Co_3O_4 (220) peak, which would have been hard to identify after cooling back to room temperature.

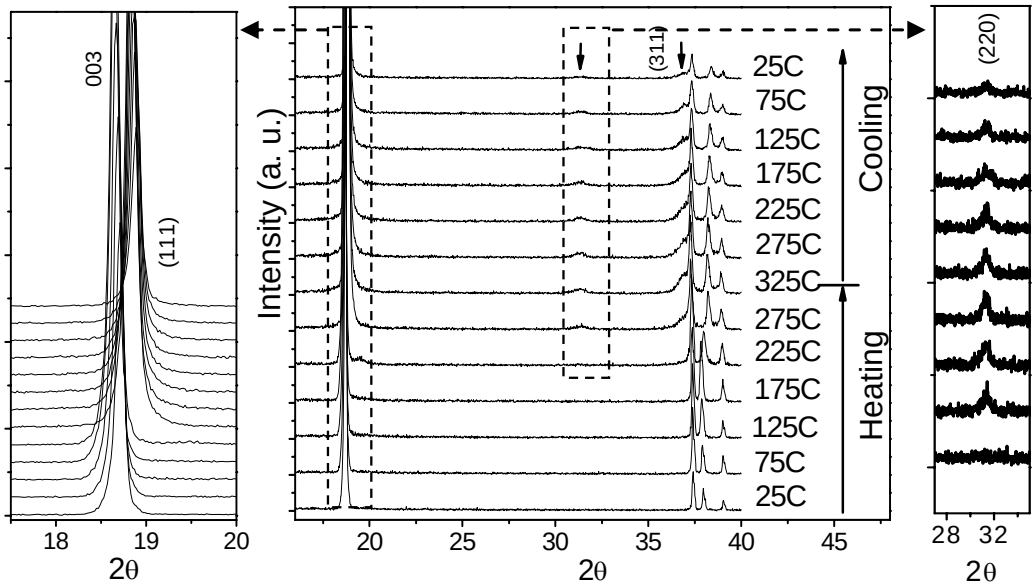

Fig. 1.6: In situ hotstage x-ray spectra of chemically delithiated $Li_{0.59}CoO_2$ synthesized by Mary Kombolias.

1.4.3 TEM

In-situ heating TEM is performed on the electrochemically delithiated specimen $Li_{0.26}CoO_2$. Analysis of the diffraction patterns could be explained by the decomposition of Li_xCoO_2 into small particles of Co_3O_4 and $LiCoO_2$ during the heat treatment. These small particles are distributed homogeneously in the matrix of the original Li_xCoO_2 particles. In Fig. 1.7 selected area electron diffraction patterns (SAD) and images taken over a time period of 2 hours at temperatures between 21°C and 300°C (nominal heating holder read out) are shown. Fig. 1.7a shows the single crystalline diffraction pattern of the starting phase $Li_{0.26}CoO_2$. At around 215°C and after 1h, the diffraction spots are smeared out and a ring pattern starts to appear (Fig. 1.7b). With time and temperature the ring pattern becomes more defined as can be seen in Fig. 1.7c taken after heating to 315°C and a total heating time of 2h. The diffraction ring pattern in Fig.1.7c indicates that many fine particles of Co_3O_4 and $LiCoO_2$ are formed, as can be seen from a comparison of the continuous rings to a indexed ring pattern for $LiCoO_2$ and Co_3O_4 (Fig 1.7d). There is no obvious change of the diffraction pattern when the specimen was cooled down to room temperature. This indicates that the reaction $Li_xCoO_2 \rightarrow LiCoO_2 + Co_3O_4$ is irreversible. A comparison between Figs. 1.7e and 1.7f, shows that the morphology distribution of small particles Co_3O_4 and $LiCoO_2$ particles has changed: After 2 hours of heating, more white phase can be seen in fig. 6f than in Fig. 1.7e.

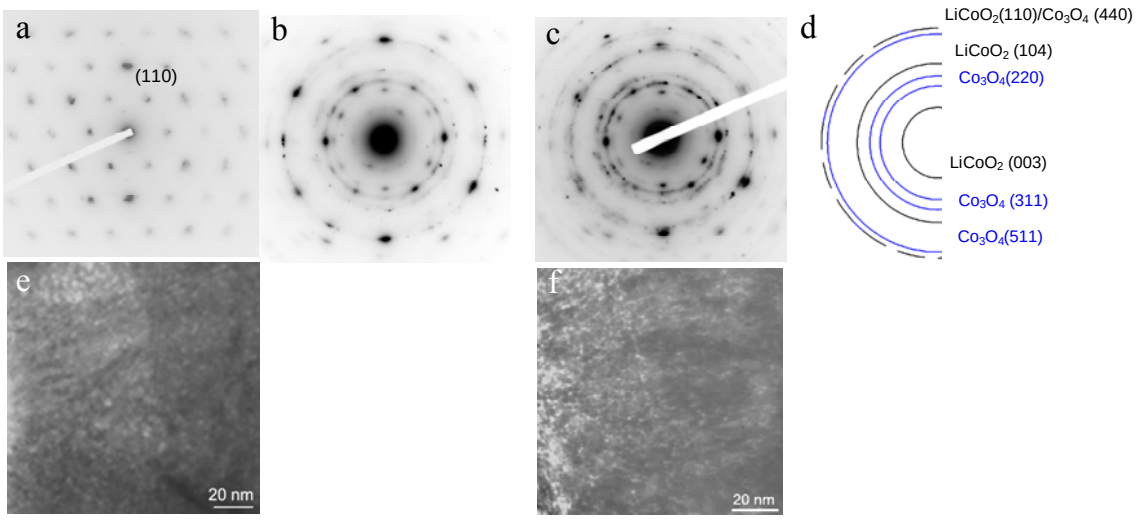

Fig. 1.7: In situ TEM of electrochemically delithated $Li_{0.26}CoO_2$. a. SAD at starting; b. SAD at 210°C after 1 h; c. SAD at 315°C after 2 hs. heating; d. index of SAD pattern c; e. image at starting; f. image at 315°C after 2 hs.

1.5 Conclusions

Up to now the P3 phase has only been reported after liquid chemical delithiation taking place at high charge rates. Here we found the P3 phase both in Li_xCoO_2 prepared chemical delithiation and by electrochemical delithiation at a high charge rate of 1C, which confirms the effect of the charge rate onto the microstructure. Heating experiments showed that Li_xCoO_2 decomposes irreversibly into fine particles of $LiCoO_2$ and Co_3O_4 at the temperature above approximate 200 ºC. The SAD patterns confirmed this decomposed reaction, and presented the process and morphology changes.

1.6 Reference

(1) Mizushima, K.; Jones, P. C.; Wiseman, P. J.; Goodenough, J. B. *Materials Research Bulletin* **1980**, *15*, 783-789.
(2) Rossen, E.; Reimers, J. N.; Dahn, J. R. *Solid State Ionics* **1993**, *62*, 53-60.

(3) Reimers, J. N.; Dahn, J. R. *J. Electrochem. Soc.* **1992**, *139*, 2091-2097.
(4) Ohzuku, T.; Ueda, A. *J. Electrochem. Soc.* **1994**, *141*, 2972-2977.
(5) Amatucci, G. G.; Tarascon, J. M.; Klein, L. C. *J. electrochem. soc.* **1996**, *143*, 1114-1123.
(6) Ven, A. V. D.; Aydinol, M. K.; Ceder, G. *Physical Review B* **1998**, *58*, 2975-2987.
(7) Chen, Z.; Lu, Z.; Dahn, J. R. *J. electrochem. soc.* **2002**, *149*, A1604-A1609.
(8) Yang, X. Q.; Sun, X.; Mcbreen, J. *electrochemistry communications* **2000**, *2*, 100-103.
(9) Gabrisch, H.; Yazami, R.; Fultz, B. *J. Power Sources* **2003**, *119-121*, 674-679.
(10) Gabrisch, H.; Yazami, R.; Fultz, B. *J. electrochem. soc.* **2004**, *151*, A891-A897.
(11) Venkatraman, S.; Manthiram, A. *Chem. Mater.* **2002**, *14*, 3907-3912.
(12) Doeff, M. M.; Hollingsworth, J.; Shim, J.; Lee, Y. J.; Striebel, K.; Reimer, J. A.; Cairns, E. J. *J. Electrochem. Soc.* **2003**, *150*, A1060-A1066.
(13) Kombolias, M. *Masters Thesis,* University of New Orleans, New Orleans, LA **2006**.

CHAPTER 2

Investigation of Cation Ordering in $LiNi_{1/3}Mn_{1/3}Co_{1/3}O_2$ by Electron Diffraction Analysis

2.1 Abstract

$LiNi_{1/3}Mn_{1/3}Co_{1/3}O_2$ is a promising new cathode material for potential applications in high power rechargeable batteries. It has a trigonal lattice of $R\bar{3}m$ symmetry, similar to that $LiCoO_2$ used in commercial batteres. The partial substitution of Co by Ni and Mn in $LiNi_{1/3}Mn_{1/3}Co_{1/3}O_2$ opens up the possibility of different cation configurations in the crystal lattice. The nickel, manganese and cobalt ions of $LiNi_{1/3}Mn_{1/3}Co_{1/3}O_2$ can be randomly distributed in the transition metal layers. Alternatively superstructures can be formed by ordering of Ni, Mn, and Co ions in the transition metal layer or by an interchange between Li and Ni ions. Selected area electron diffraction patterns were collected from pristine $LiNi_{1/3}Mn_{1/3}Co_{1/3}O_2$ and from $LiNi_{1/3}Mn_{1/3}Co_{1/3}O_2$ charged to 5.2 V that was disassembled in the discharged state. We found that the $LiNi_{1/3}Mn_{1/3}Co_{1/3}O_2$ investigated here (ENAX, Inc.) is inhomogeneous with respect to morphology and cation ordering. 15 randomly selected particles of the pristine material were investigated by electron diffraction. The selection contains single crystalline (66.7%) and polycrystalline particles (33.3%). In six out the 15 particles (40%) we observe superlattice reflections. After charging to a high voltage of 5.2 V followed by discharge, we found fewer particles with superlattices (10%) than in the virgin sample. Some diffraction

patterns containing superlattice reflections can be explained by $\sqrt{3}a_{Hex} \times \sqrt{3}a_{Hex} \times c_{Hex}$ supercell with $P3_112$ symmetry.

Keywords: $LiNi_{1/3}Mn_{1/3}Co_{1/3}O_2$; electron diffraction pattern; superlattice.

2.2 Introduction

Lithium-ion batteries offer high energy density compared to other rechargeable systems. They have become an attractive and important energy storage source for portable electronic devices as demand for mobile power sources increases. Lithium cobalt oxide ($LiCoO_2$) has played an important role in the family of lithium-ion batteries since it has been first reported by Goodenough.[1] Recently, layered lithium nickel manganese oxides ($LiNi_{0.5}Mn_{0.5}O_2$) and $LiNi_{1/3}Mn_{1/3}Co_{1/3}O_2$ have been considered as promising, inexpensive, and nontoxic intercalation compounds for the positive electrode replacing $LiCoO_2$. A capacity of 200 $mAhg^{-1}$ has routinely been achieved at low rates in $LiNi_{0.5}Mn_{0.5}O_2$ based cathodes when the cells were operated at 2.5-4.5V.[2-5] This is higher than the practical capacity of 150 $mAhg^{-1}$ for $LiCoO_2$, though both have almost the same theoretical capacity of 280 $mAhg^{-1}$. High ordered $LiNi_{0.5}Mn_{0.5}O_2$ with excellent electrochemical properties, compared to $LiNi_{0.5}Mn_{0.5}O_2$ produced by the solid-state method can be produced by an ion-exchange method.[6] Both theoretical and experimental studies have been performed to understand the crystal structure,[7,8] cation ordering,[9,10] and phase transitions of $Li_xNi_{0.5}Mn_{0.5}O_2$,[11] and the effect of high voltage charging on the structure and electrochemistry of $LiNi_{0.5}Mn_{0.5}O_2$.[12] $LiNi_{1/3}Mn_{1/3}Co_{1/3}O_2$, which was first proposed by Ohzuku and Makimura,[13] has attracted a great deal of interest as a possible replacement for $LiCoO_2$. The advantages of $LiNi_{1/3}Mn_{1/3}Co_{1/3}O_2$ over $LiCoO_2$ include excellent rate capability, superb cycling performance, and good thermal stability. Upon heating an exothermic peak is observed in $LiCoO_2$ around 220

˚C, while in $LiNi_{1/3}Mn_{1/3}Co_{1/3}O_2$ the exothermic peak is observed at a temperature above 270 ˚C using DSC.[14] The better thermal stability of $LiNi_{1/3}Mn_{1/3}Co_{1/3}O_2$ makes it safer than $LiCoO_2$ in applications. The chemical and structural behavior of $LiNi_{1/3}Mn_{1/3}Co_{1/3}O_2$ is superior to that of $LiCoO_2$. The $Li_{1-x}Ni_{1/3}Mn_{1/3}Co_{1/3}O_2$ system is chemically stable for (1-x) > 0.35 without oxygen loss and structurally stable for (1-x) > 0.23 by maintaining O3 structure.[15] For comparison Li_xCoO_2 is stable in the lithium content range $1 < x < 0.5$.[16] [17] There is no big difference in theoretical capacity between $LiNi_{1/3}Mn_{1/3}Co_{1/3}O_2$ and $LiCoO_2/LiNi_{0.5}Mn_{0.5}O_2$. However, $LiNi_{1/3}Mn_{1/3}Co_{1/3}O_2$ has the higher practical rechargeable capacity than others. The practical rechargeable capacity of $LiNi_{1/3}Mn_{1/3}Co_{1/3}O_2$ is 160 $mAhg^{-1}$ in the potential window of 2.5-4.4 V and more than 200 $mAhg^{-1}$ in the voltage range of 2.8-4.6 V.[18,19] 4.3 V was reported to be a proper upper cutoff voltage for $LiNi_{1/3}Mn_{1/3}Co_{1/3}O_2$ cathode material. The capacity faded obviously when cells with $LiNi_{1/3}Mn_{1/3}Co_{1/3}O_2$ cathodes were charged to voltages higher than 4.3 V.[19] According to first principle calculations, $LiNi_{1/3}Mn_{1/3}Co_{1/3}O_2$ is not a solid solution of $LiCoO_2$, $LiNiO_2$ and $LiMnO_2$ because both $LiCoO_2$ and $LiNiO_2$ are immiscible with $LiMnO_2$.[20] The formal charges of Co, Ni, and Mn in $LiNi_{1/3}Mn_{1/3}Co_{1/3}O_2$ are +3, +2, and +4, respectively, investigated by first-principles calculation,[21,22] solid-state nuclear magnetic resonance (NMR), and X-ray absorption spectroscopy (XAS).[23,24] The charge compensation during charge of the battery is achieved by oxidation of Ni^{2+}/Ni^{4+} and Co^{3+}/Co^{4+} as well as in the oxygen site. Manganese ions remain mostly unchanged in the Mn^{4+} state. The crystal structure of $LiNi_{1/3}Mn_{1/3}Co_{1/3}O_2$ can be described by the hexagonal α-$NaFeO_2$ structure with $R\bar{3}m$ symmetry. Different synthesis conditions were employed to fabricate $LiNi_{1/3}Mn_{1/3}Co_{1/3}O_2$, such as hydroxide co-precipitation method and various annealed temperatures, and effects of synthesis on the structural and electrochemical properties were tested.[19,25-29] Nonstoichiometric

$LiNi_{1/3}Mn_{1/3}Co_{1/3}O_2$ compounds with lithium-excess or Li vacancies have also been investigated in an attempt to improve the electrochemical properties[30,31] and to understand the de-intercalation mechanism.[32] Electrochemical performance and cycling behavior were improved by adding LiF to the active material,[33,34] by metal oxide coating, [35] and even mixing $LiCoO_2$/ $LiNi_{1/3}Mn_{1/3}Co_{1/3}O_2$ as active cathode material.[36]

Superstructures within the parent phase space group of $R\bar{3}m$ have been reported for $LiNi_{0.5}Mn_{0.5}O_2$ and $LiNi_{1/3}Mn_{1/3}Co_{1/3}O_2$.[8-12] The crystal and the electronic structures of $LiNi_{1/3}Mn_{1/3}Co_{1/3}O_2$ have been investigated by theoretical and experimental methods in order to understand the formation of superstructures.[15,20-24,37] The replacement of cobalt by two transition metal species in $LiNi_{1/3}Mn_{1/3}Co_{1/3}O_2$ opens the possibility for different elemental distributions of cations among the available lattice sites. Assuming a cation distribution with maximum distance between ions of the same species a $[\sqrt{3}\times\sqrt{3}]R30^0$ model can be developed for in plane ordering. Alternatively a pile-up model has been considered in which Co, Mn and Ni occupy separate TM layers.[21,22] The lattice parameters of $LiNi_{1/3}Mn_{1/3}Co_{1/3}O_2$ from calculations (a = 2.831 Å, c = 13.88 Å for $[\sqrt{3}\times\sqrt{3}]R30^0$ model; a = 2.827 Å, c = 13.94 Å for piled-up model) are smaller than those determined from experiments (a = 2.867 Å, c = 14.246 Å).[13,22] Theoretical calculations based on the application of local spin density approximation (LSDA) showed that the formation energy for the $[\sqrt{3}\times\sqrt{3}]R30^0$ model is -0.17 eV, compared to +0.06 eV for the piled-up model in. Therefore, the $[\sqrt{3}\times\sqrt{3}]R30^0$ model is a preferable superlattice to form during processing of $LiNi_{1/3}Mn_{1/3}Co_{1/3}O_2$. Local atomic characterization of $LiNi_{1/3}Mn_{1/3}Co_{1/3}O_2$ by x-ray absorption fine structure (XAFS) measurements showed results in good agreement with the superlattice model of $[\sqrt{3}\times\sqrt{3}]R30^0$ type.[24] On the other hand, Whitfield et al found a

random distribution of Mn, Ni, and Co over the 3a sites in the $R\bar{3}m$ structure based on neutron and anomalous dispersion powder diffraction results.[37] No experimental evidence of a superlattice was presented in that paper.

Here we use electron diffraction in transmission electron microscopy (TEM) to study the crystal structure of $LiNi_{1/3}Mn_{1/3}Co_{1/3}O_2$ particles. Both virgin and cycled $LiNi_{1/3}Mn_{1/3}Co_{1/3}O_2$ specimens were investigated. The cycled specimen was charged to 5.2 V and then discharged in order to understand the effect of charging to high voltage on the material structure. Our results show that the material is inhomogeneous. It consists of single and polycrystalline particles. In samples from the pristine and the charged/discharged cathode we find a difference in the fraction of crystal lattices with cation ordering in the TM layers.

2.3 Experiments

Cycled $LiNi_{1/3}Mn_{1/3}Co_{1/3}O_2$ used in this study was obtained in the form of cathodes from R. Yazami at the California Institute of Technology. They prepared lithium half cells and performed the charge and discharge processes. The pristine $LiNi_{1/3}Mn_{1/3}Co_{1/3}O_2$ (a = 2.867Å, c = 14.246Å) powder was obtained courtesy of Enax. Inc. and was synthesized following the recipe published by Ohzuku.[13] Here we compare pristine $LiNi_{1/3}Mn_{1/3}Co_{1/3}O_2$ to $LiNi_{1/3}Mn_{1/3}Co_{1/3}O_2$ charged to 5.2 V after 5 formation cycles between 2.5 and 4.5 V. The cycled specimen is studied in the discharged state.

X-ray diffraction using a Philips X'-Pert diffractometer using Cu Kα radiation (λ = 1.54 Å) and electron diffraction were used to characterize $LiNi_{1/3}Mn_{1/3}Co_{1/3}O_2$ specimens. X-ray diffraction patterns (XRD) for cycled specimens came from the cathodes, which were immediately disassembled from cycled half-cells after discharge. For TEM specimen preparation

the mixture of active material, carbon black and binder was scraped off the cathodes, washed repeatedly in diethyl carbonate (DEC), 1-methyl-2-pyrrolidone (NMP), followed by a wash in ethanol. The suspension with ethanol was transferred onto a holey carbon grid. TEM studies were performed on the JEOL2010 TEM at AMRI of the University of New Orleans operated at 200 kV.

Electron diffraction patterns were simulated using the programs Desktop Microscopist and JEMS. X-ray and neutron diffraction patterns were simulated with the program PowderCell. The structural sketch of $LiNi_{1/3}Mn_{1/3}Co_{1/3}O_2$ with $P3_112$ symmetry was drawn with the program CrystalMaker. $LiCoO_2$ structure with the parameters of $LiNi_{1/3}Mn_{1/3}Co_{1/3}O_2$ (a = 2.867Å, c = 14.246Å)[13] was used to simulate O3 phase of $LiNi_{1/3}Mn_{1/3}Co_{1/3}O_2$ (Table 2.1). Disordered Ni, Mn and Co atoms occupy the Co sites to form O3 phase of $LiNi_{1/3}Mn_{1/3}Co_{1/3}O_2$. Therefore, we can use Co atom to substitute the other atoms in the simulations. The structural parameters of superstructure $P3_112$ used in the simulations were listed in table 2.2.[13,21]

Table 2.1: structural parameters used to simulate O3 phase of $LiNi_{1/3}Mn_{1/3}Co_{1/3}O_2$ (No. 166). a = 2.867Å, c = 14.246Å [Ref. 13, 17]

Element	Wyckoff	x	y	z
Li	3a	0	0	0
Co/Ni/Mn	3b	0	0	0.5
O	6c	0	0	0.2395

Table 2.2: structural parameters used to simulate $LiNi_{1/3}Mn_{1/3}Co_{1/3}O_2$ superstructure $P3_112$ (No. 151). a = 2.867Å, c = 14.246Å [Ref. 13, 21]

Element	Wyckoff	x	y	z
Li(1)	3b	0.7785	0.8892	0.5
Li(2)	3b	0.1178	0.5589	0.5
Li(3)	3b	0.4348	0.2174	0.5
Co	3a	0.7773	0.8886	0
Ni	3a	0.1106	0.5553	0
Mn	3a	0.4457	0.2228	0
O(1)	6c	0.7950	0.9020	0.2564
O(2)	6c	0.0977	0.5589	0.2553
O(3)	6c	0.4402	0.2046	0.2558

2.4 Results

2.4.1 Pristine $LiNi_{1/3}Mn_{1/3}Co_{1/3}O_2$

2.4.1.1 Single crystals with $R\bar{3}m$ space group

Selected Area Electron diffraction (SAED) patterns were collected from 15 randomly selected crystals in the pristine sample $LiNi_{1/3}Mn_{1/3}Co_{1/3}O_2$. Ten out of 15 (66.7%) particles were homogenous single crystal. Figs. 2.1a, b show an image of a homogeneous particle and its electron diffraction pattern. The same SAED pattern at $[\bar{4}401]$ zone axis orientation was obtained at every selected area on this particle. Fig. 2.1c shows the high resolution transmission electron microscopy (HRTEM) image of a $LiNi_{1/3}Mn_{1/3}Co_{1/3}O_2$ particle. The spacing between (0001) planes is 4.74Å measured in this image using the nominal magnification of the instrument. The c lattice parameter calculated from this image is 14.22 Å, which is in good agreement with reported literature values.[13]

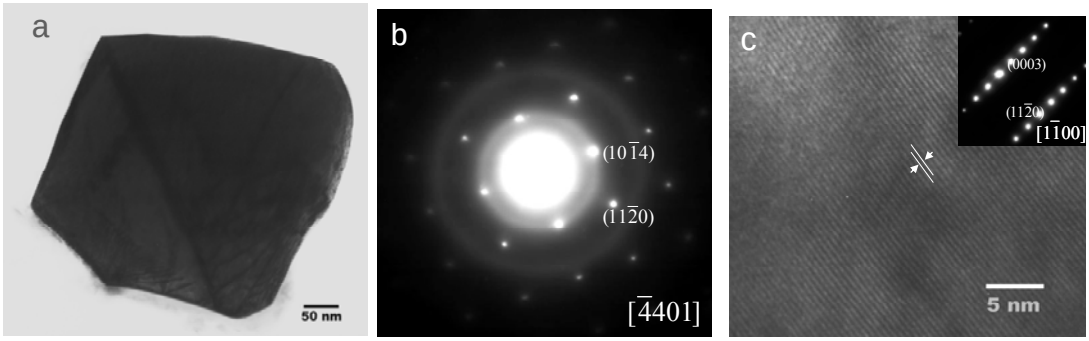

Fig. 2.1: Single crystal with $R\bar{3}m$ symmetry a) image of a single crystal; b) the electron diffraction pattern for a; c) a high resolution image at $[1\,\bar{1}00]$ zone.

2.4.1.2 Polycrystalline crystals with $R\bar{3}m$ space group

Five out of 15 (33.3%) particles were polycrystalline crystals. One example is given below. Different SAD patterns were collected from different areas of this particle. Obviously, this particle is made up of several crystals in various orientations. The pattern shows in Fig. 2.2c is a superposition of a diffraction pattern of the O3 phase in zone axis orientation $[02\bar{2}1]$ and $[2\,\bar{1}\,\bar{1}0]$. The $\{11\bar{2}0\}$ and $\{\bar{1}104\}$ reflections of the <0221> pattern coincide with the $\{1\,\bar{1}08\}$ and $\{1\,\bar{1}04\}$ reflections of the pattern in <2110> orientation leading the appearance of strong reflections. The electron diffraction pattern in Fig. 2.2d contains three patterns namely in $[2\,\bar{1}\,\bar{1}0]$, $[\bar{2}110]$ and $[02\bar{2}1]$ zone axis orientation. The strong reflections in pattern d are the result of superposition. The SAD patterns b and e came from crystals in $[02\bar{2}1]$ and$[\bar{2}110]$ orientation. The electron diffraction patterns b1,c1,e1 are simulated patterns using Desktop Microscopist.

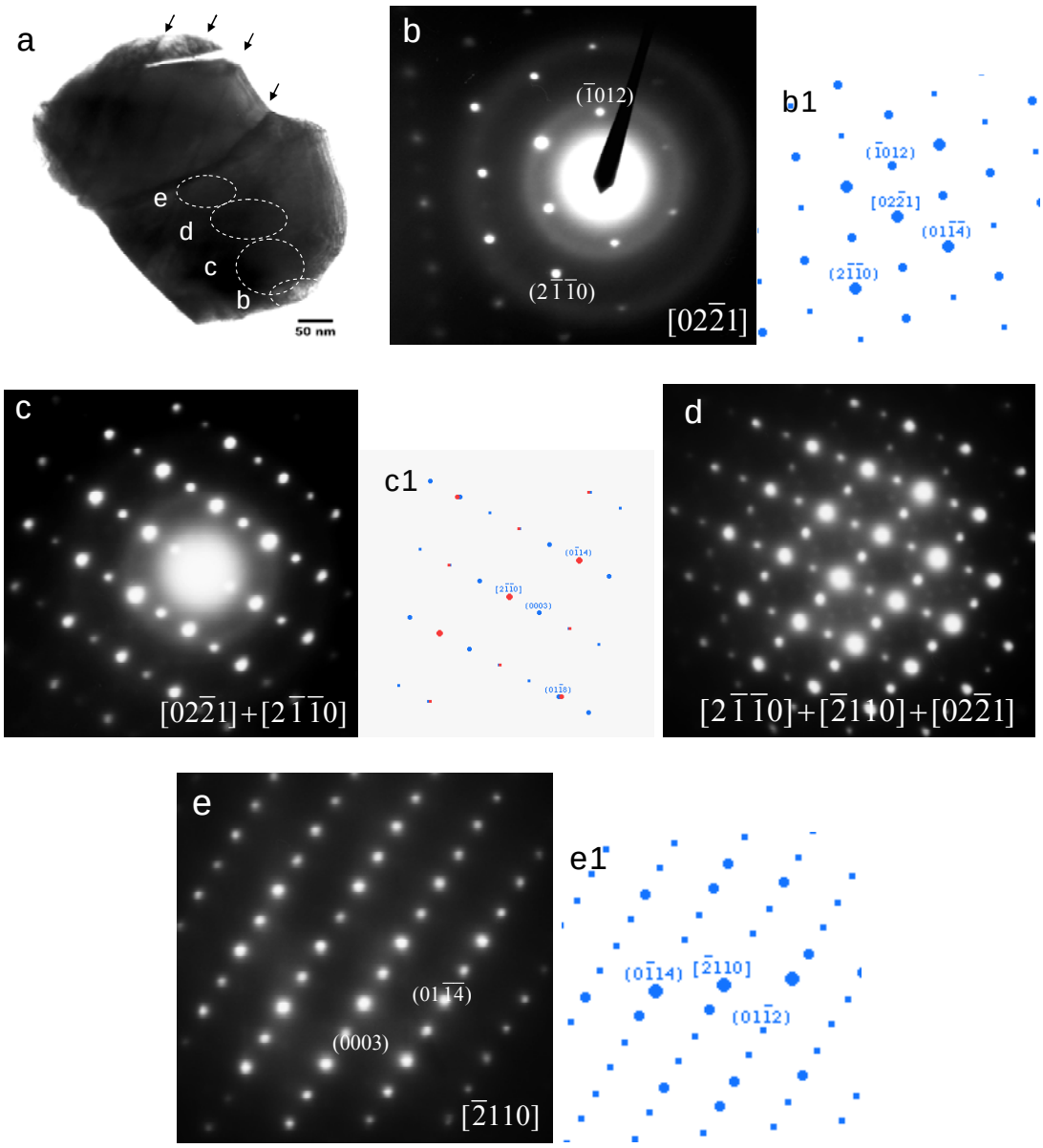

Fig.2.2: Image and diffraction patterns of a polycrystal. a) the selections from where the diffraction patterns have been taken are marked by b, c, d, e; b) an electron diffraction pattern in zone axis orientation $[02\bar{2}1]$; c) electron diffraction pattern at c showing a superposition of two electron diffraction patterns in zone axis orientation $[02\bar{2}1]$ and $[2\bar{1}\bar{1}0]$; d) electron diffraction pattern at d showing a superposition of three electron diffraction patterns at zone axis orientations $[2\bar{1}\bar{1}0]$, $[\bar{2}110]$ and $[02\bar{2}1]$; e) an electron diffraction pattern at zone axis orientation $[\bar{2}110]$; b1, c1, e1) simulated patterns corresponding to b, c, e using Desktop Microscopist.

2.4.1.3 Superlattices

Six out of 15 (40%) particles had new reflection spots that don't appear in patterns of the O3 phase. Some of these can be explained assuming a superlattice as proposed by Koyama et al.[22] Fig. 2.3b shows the SAED pattern in [0001] zone axis orientation collected from a particle showing in Fig. 2.3a. Fig. 2.3b1 shows a simulated SAED pattern of the $[\sqrt{3}\times\sqrt{3}]R30^0$ superlattice structure in [0001] orientation. A comparison shows that the weak reflections that appear between the fundamental (300) reflections in the experimental pattern are reproduced in the simulated pattern. We call this type of pattern case A. The two most predominant features observed in the remaining particles showing extra reflections are the appearance of extra spots perpendicular to $(11\bar{2}0)$ type planes (see Figs. 2.3d, 2.3f) and the observation of new spots halfway between $(\bar{1}102)$ type reflections (see Fig. 3h). The particles from which the electron diffraction pattern in Fig. 2.3d, f, h are taken are shown in Fig. 2.3c, e, g, respectively. In the SAED pattern shown in Fig. 2.3d, three weak spots can be observed between each $\{11\bar{2}0\}$ type reflection. A similar observation is shown in Fig. 2.3f in an electron diffraction pattern in $[\bar{4}401]$ zone axis orientation. The new reflections are separated by 1/6 of the distance between 2 $\{11\bar{2}0\}$ type reflections and are centered between 2 $\{11\bar{2}0\}$ reflections. The distances between the extra spots suggest a superlattice at sixfold distance between $\{11\bar{2}0\}$ planes. However, in both cases only 3 and not 5 extra reflections are observed. Therefore, at this time we have no conclusive evidence for the formation of a superlattice cell. We call this type case B. The electron diffraction patterns in Fig. 2.3h, i, collected from the particle in Fig. 3g, show new reflections halfway between $\{11\bar{2}0\}$ and $\{\bar{1}102\}$ type reflections in the $[\bar{1}101]$ zone axis orientation patterns. The electron diffraction pattern in Fig. 2.3i has been taken from the edge of the particle

(marked by ‘i’ in Fig. 2.3g). A comparison between Fig. 2.3h and 2.3i shows that the reflections in Fig. 2.3i have streaks. We call diffraction patterns with new reflections halfway between fundamental reflections case C. All together we observed 2 particles of case A, 3 particles of case B and 1 particle case C.

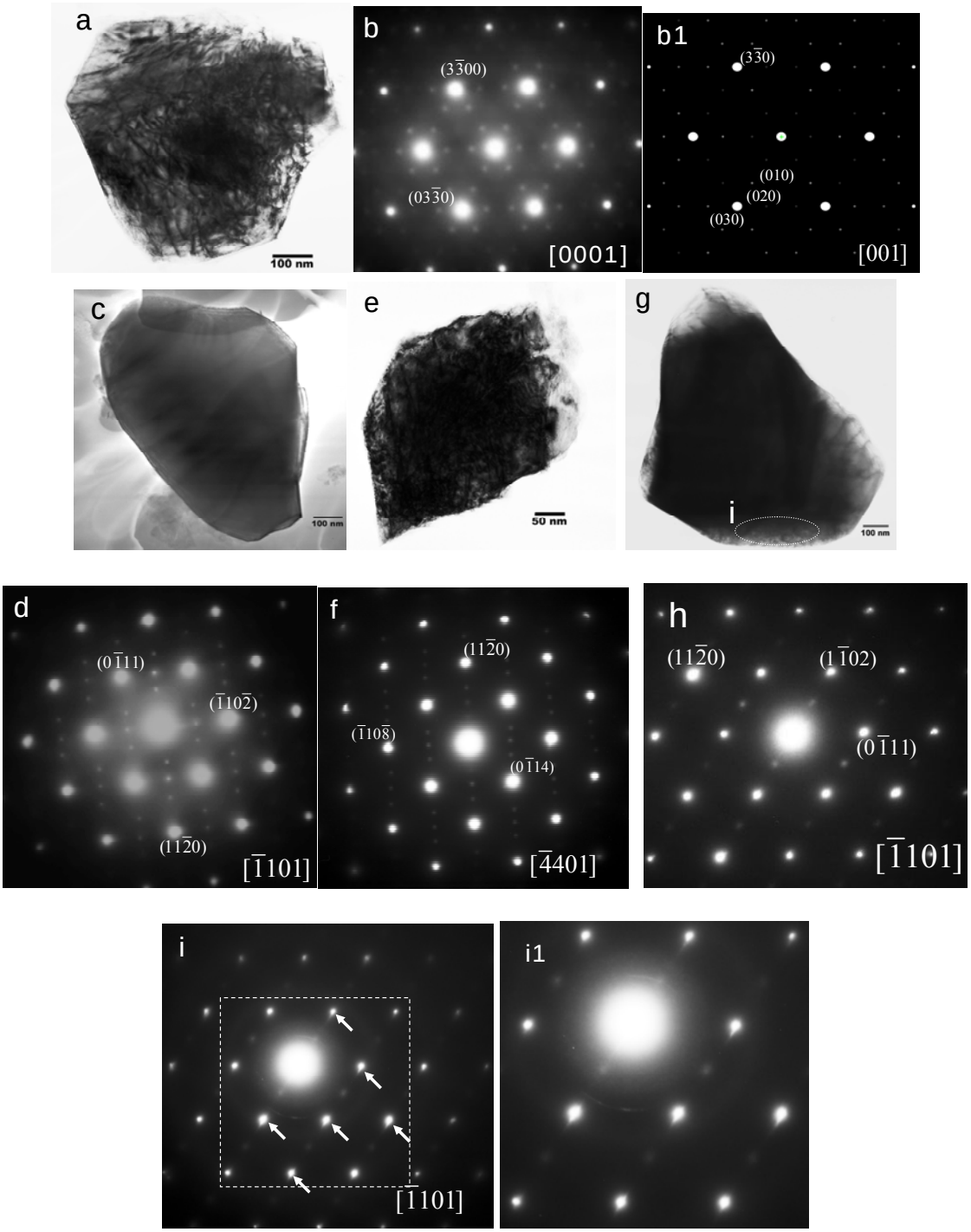

Fig. 2.3: Images and SAED patterns of superlattices a) an image for a particle with superlattices; b) a diffraction pattern at zone [0001] of $P3_112$ for particle in (a); b1) a corresponding simulation diffraction pattern of b by JEMS program; c), e), g) particles with superlattices; d), f), h) the electron diffraction pattern at zone [$\bar{1}$101], [$\bar{4}$401], [$\bar{1}$101] for particles in (c), e), g), respectively; i) a diffraction pattern from selected area i in image g; i1) enlarged part of i diffraction pattern showing streaking.

2.4.2 Cycled specimen at discharged state

In the particles retrieved from the cathode charged to 5.2 V we made similar observations as in the pristine $LiNi_{1/3}Mn_{1/3}Co_{1/3}O_2$. However, the number of diffraction patterns with extra reflections was much smaller than in the virgin specimen. Twenty randomly selected particles were investigated by TEM. Only two out of 20 (10%) had extra reflection spots in the diffraction patterns; the others could be indexed in space group $R\bar{3}m$ and were either single crystals or polycrystalline particles with the space group $R\bar{3}m$ (10/20 single crystals and 8/20 polycrystalline crystals). These two particles with extra reflection spots in diffraction patterns are both in case C. One example of a pattern with superlattice reflection is given in Fig. 2.4.

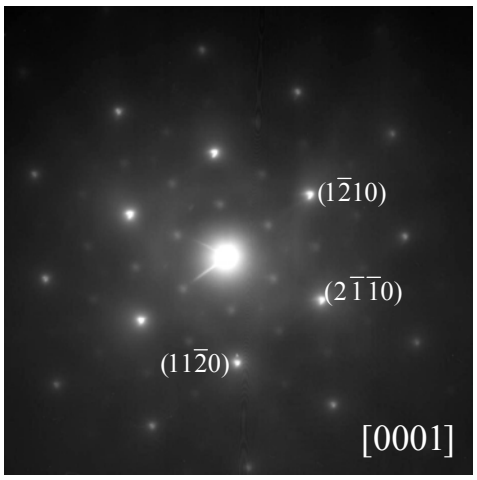

Fig. 2.4: an electron diffraction pattern at [0001] zone axis showing superlattice reflections.

Fig. 2.5 is showing a X-ray diffraction spectrum of the specimen charged to 5.2 V at discharge state. The spectrum was indexed as O3 phase. The noise of the background come from

the impurity (carbon, aluminum, et al.) of the cathode since this X-ray spectrum was taken directly from the cathode with aluminum foil.

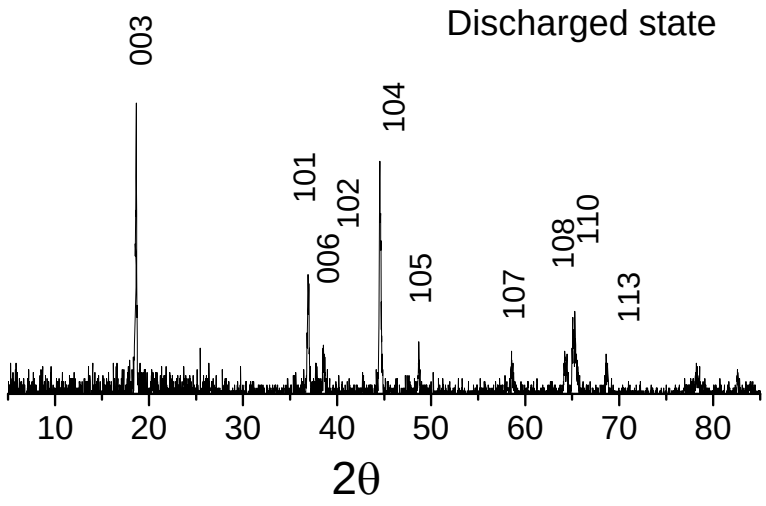

Fig. 2.5: X-ray diffraction spectrum of $LiNi_{1/3}Mn_{1/3}Co_{1/3}O_2$ charged to 5.2 V at discharge state.

2.5 Discussion

2.5.1 Morphology

The observed particles can be classified as single and polycrystalline crystals. Considering that the material was produced from a solid state method using $LiOH{\cdot}H_2O$, $CoCO_3$, and a nickel manganese hydroxide as starting material[13], we can only speculate that one of the precursor was polycrystalline, or that several crystals have joined together during heating to form a polycrystal.

2.5.2 Cations ordering

The phases of $LiNi_{1/3}Mn_{1/3}Co_{1/3}O_2$ are more complex than its parent $LiCoO_2$ since cobalt is replaced by three transition metals (TM) in this generation. When only cobalt ions occupy the transition metal layer, the result is $R\bar{3}m$ symmetry for virgin $LiCoO_2$. Different distributions of three transition metals in $LiNi_{1/3}Mn_{1/3}Co_{1/3}O_2$ will change the symmetry of the resulting lattice. Furthermore, it is well known that nickel ions exchange positions with lithium ions easily due to their similar radii.[38] We begin by considering the distributions of Ni, Mn, and Co ions in TM layer at 3a sites in $R\bar{3}m$. If the three cations are distributed randomly in the TM layer, a diffraction pattern corresponding to that of $LiCoO_2$ in $R\bar{3}m$ symmetry is obtained. If two cations of the same species assume the largest periodical distance, and each cations is surrounded by cations of the other two species in the TM layer, a $[\sqrt{3}\times\sqrt{3}]R30^0$ structure with space group $P3_112$ as introduced by Koyama will be formed.[22] (Fig. 2.6). The Ni, Mn, and Co cations occupy octahedral sites in TM layers (Fig. 2.6b) with $\sqrt{3}a_{Hex.}$ distance between two atoms of one species (Fig. 2.6c). Alternatively to the $\sqrt{3}a_{Hex.}\times\sqrt{3}a_{Hex.}$ in plane ordering of Ni, Mn, and Co, one could assume that each species occupies a separate TM layer in the unit.[22] We have simulated the electron diffraction patterns that correspond to both cases, using unit cell listed in table 2.2 and modified unit cell for the pile-up model (listed in the appendix A). We also simulated the case of Ni and Li interchange between respective layers for $[\sqrt{3}\times\sqrt{3}]R30^0$ model (unit cell given in appendix B) and O3 model (appendix C). In Fig. 2.7 the [001] zone axis patterns for the three cases and [112] zone axis pattern for spinel structure are shown. In the majority of particles analyzed here, we find diffraction patterns that are in agreement with the $R\bar{3}m$ of $LiCoO_2$ indicating that the Ni^{2+}, Co^{3+}, Mn^{4+} are randomly distributed on 3a sites in TM layers.

The formation of superstructure has been reported in the generations of $LiCoO_2$ such as $LiNi_{0.5}Mn_{0.5}O_2$ and $LiNi_{1/3}Mn_{1/3}Co_{1/3}O_2$ cathode materials.[8,11,12,22] The ordered distributions of transition metallic ions and the Li/Ni disorder contribute differently to the formation of superstructures, translating into different extra reflections in the corresponding electron diffraction patterns (see our simulations in Figs. 2.7). Experimental evidence for the models used in Figs. 2.7 are shown in Figs.2.3 and Figs. 2.4. A comparison between experimental and simulated diffraction patterns shows that the experimentally observed case A corresponds to the $\sqrt{3}a_{Hex.} \times \sqrt{3}a_{Hex.}$ in plane ordering suggested by Koyama (Fig. 2.3b). Case C corresponds to a model considering Li and Ni interchange (Fig. 2.3h, i). No experimental evidence could be found for pile-up model assuming that Co, Ni, and Mn occupy separate TM layers. A comparison between Figs. 2.3d and 2.3h shows that in both patterns new reflections are observed halfway between the fundamental $\{11\bar{2}0\}$, $\{1\bar{1}02\}$ reflections which corresponds to case C. However, in Fig. 2.3d these new reflections are surrounded by a pair of satellite reflections that are not reproduced by our models. Satellite reflections can be caused by modulations in the chemical composition (e.g. spinodal decomposition), periodic arrays of planar defects or small inclusions. In literature similar electron diffraction patterns were reported for $LiMn_{0.5}Ni_{0.5}O_2$. These patterns were explained by a $2\sqrt{3} \times 2\sqrt{3}a_{Hex.}$ superstructure[9,11,38] as well as by a specific stacking order of the so-called flower structure indicating that their origin is not completely understood at present. We leave case B unresolved for the time being.

A comparison between the number of particles having superstructures in the pristine (40%) and the cycled (10%) $LiNi_{1/3}Mn_{1/3}Co_{1/3}O_2$ shows that fewer particles with superstructure are observed in the latter. We speculate that nickel migration upon cycling is the reason for less frequent observation of superlattice reflections after cycling. It is well known that some Li can be

found in the TM layers of these compounds. Upon charge of the batteries lithium ions are removed from both Li-rich and TM-rich layers opening up empty lattice sites for nickel ions from lithium-rich layers. The nickel ions can occupy both octahedral and tetrahedral sites. Very early in the charge process Li-ions are removed from TM layers, enabling Ni diffusion to these sites. During charge to higher voltages more Li are removed from the lattice.[10,12] In return, more nickel ions migrate from Li layers to TM layers at high voltage. Only some of those nickel ions will return to the Li layers during discharge process. Therefore, Li/Ni disorder in cycled specimen is less than virgin specimen. Additionally, as a result of the nickel ion migrations to the TM layers, the ordering of nickel, manganese and cobalt in TM layers becomes disturbed. These two contributions are likely reasons why fewer superstructures are observed in cycled $LiNi_{1/3}Mn_{1/3}Co_{1/3}O_2$ than in pristine powder.

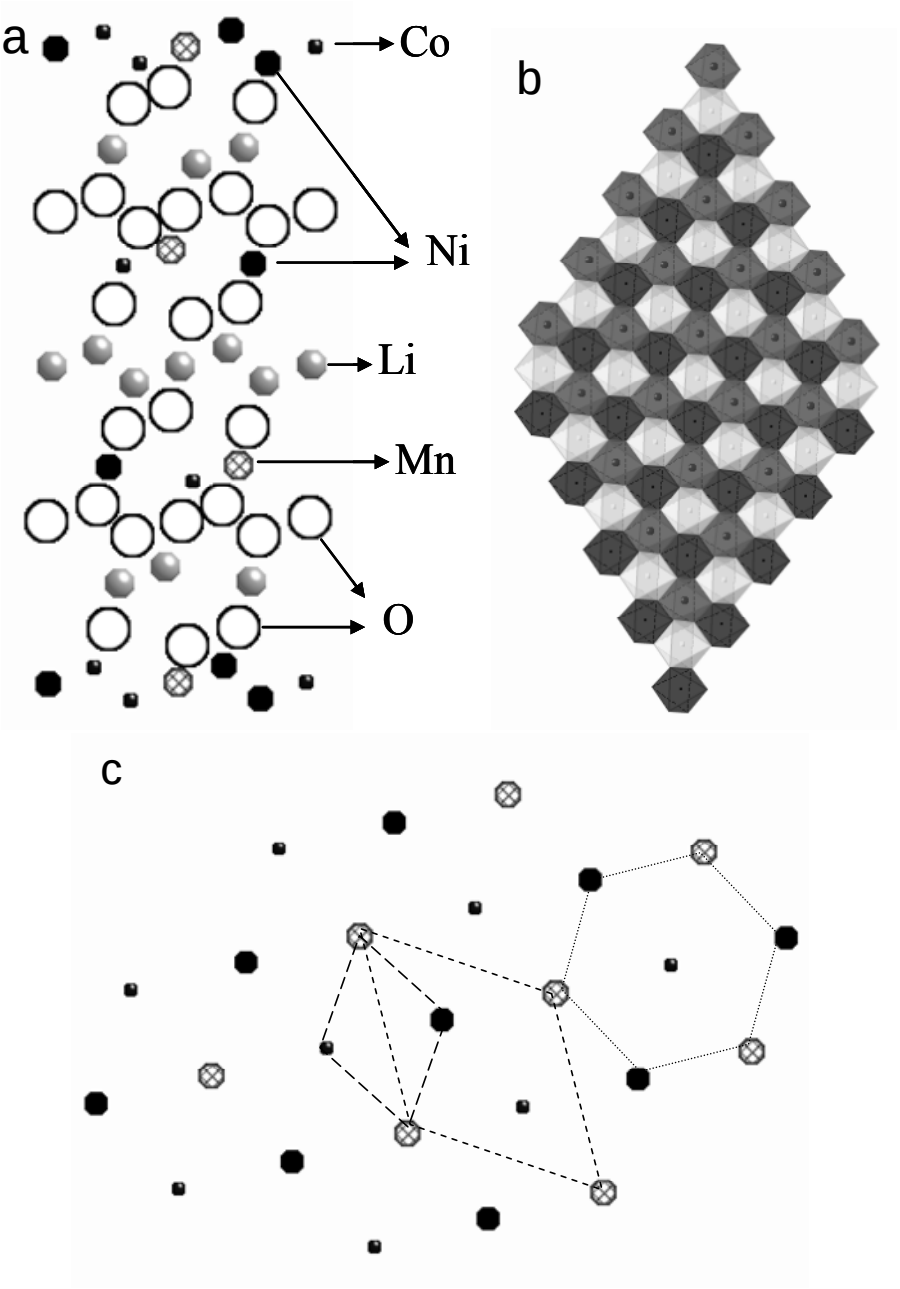

Fig. 2.6: Structures of $LiNi_{1/3}Mn_{1/3}Co_{1/3}O_2$ a) The schematic structure of $LiNi_{1/3}Mn_{1/3}Co_{1/3}O_2$ with $P3_112$ space group; b) polyhedral structure of TM layer; c) the arrangement of Ni, Mn, Co in TM layers.

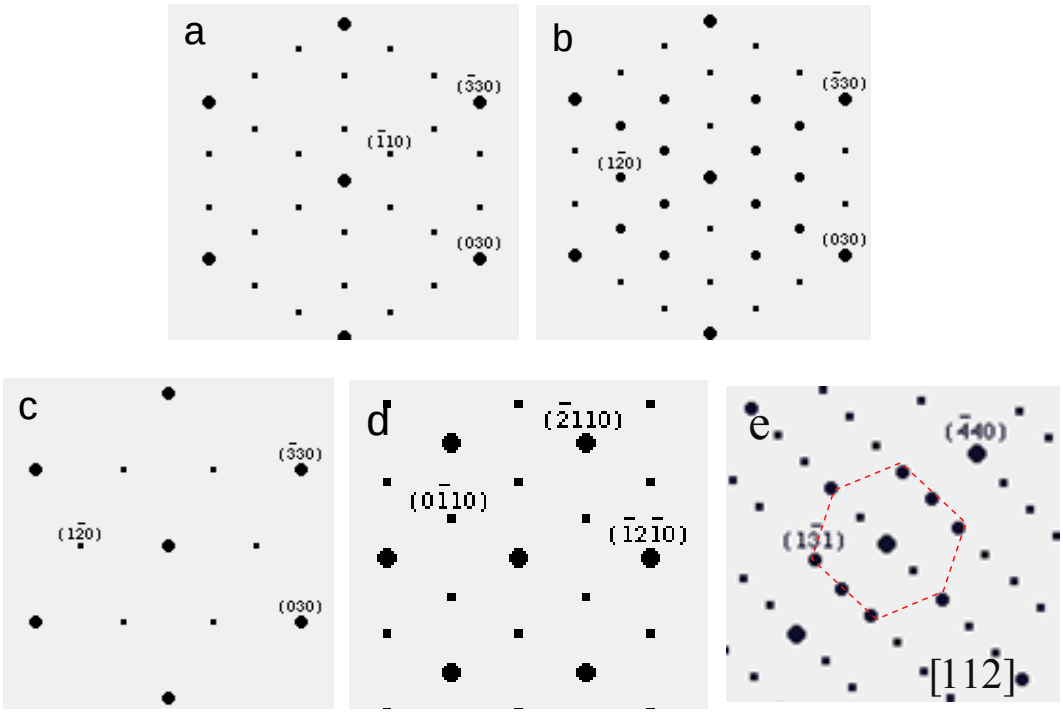

Fig. 2.7: simulated SAED patterns a) Diffraction pattern at zone axis orientation [001] for a $[\sqrt{3}\times\sqrt{3}]R30^0$ model; b) Diffraction pattern at zone axis orientation [001] for $[\sqrt{3}\times\sqrt{3}]R30^0$ model with partial Li/Ni interchange; c) Diffraction pattern at zone axis orientation [001] for pile-up model; d) Diffraction pattern at zone axis orientation [0001] for O3 model with partial Li/Ni interchange; e) spinel pattern at zone axis [112] with some Ni at tetragonal sites. All these SAED patterns are simulated using Desktop Microscopist.

2.5.3 X-ray and neutron diffraction simulations

Structures with space group $P3_112$ and $R\bar{3}m$ can be identified by neutron diffraction instead of X-ray diffraction. Nickel, manganese, and cobalt ions have similar electron configurations, which results in similar X-ray signals. The X-ray diffraction patterns of $P3_112$ and $R\bar{3}m$ structures showing in Fig. 2.8 It can be seen that they are almost the same. The superlattice peak intensities are relative 1% of the intensity of fundamental (003) peak, which are showing in the enlarged spectrum from 20˚-35˚. The very low intensity superlattice peaks are

hardly observed and identified experimentally. The disorder of Li/Ni distribution has a negligible effect on the superstructure reflection intensity.[8] In conclusion, x-ray diffraction technique is not good to detect superlattices formed by both ordering of Ni^{2+}, Mn^{4+} and Co^{3+} in TM layer and disorder of Li/Ni ions. However, these metallic ions in $LiNi_{1/3}Mn_{1/3}Co_{1/3}O_2$ have significantly different neutron scattering lengths (b_{Ni} = 10.3 fm; b_{Mn} = -3.73 fm; b_{Co} = -6.2 fm; b_{Li} = -1.9 fm). Therefore, the neutron diffraction pattern of the ordered transition metallic ions in TM layer $[\sqrt{3}\times\sqrt{3}]R30^0$ structure with space group $P3_112$ is distinctly different from the one of $R\bar{3}m$ structure with random TM ions distribution (Fig. 2.9). Bear in mind, Li occupancy on the Ni site could significantly lower the contrast of different sites in the TM layers in powder neutron diffraction patterns. Then the intensities of superstructure reflections from Li/Ni disorder contribution could be low enough to be undetectable experimentally.

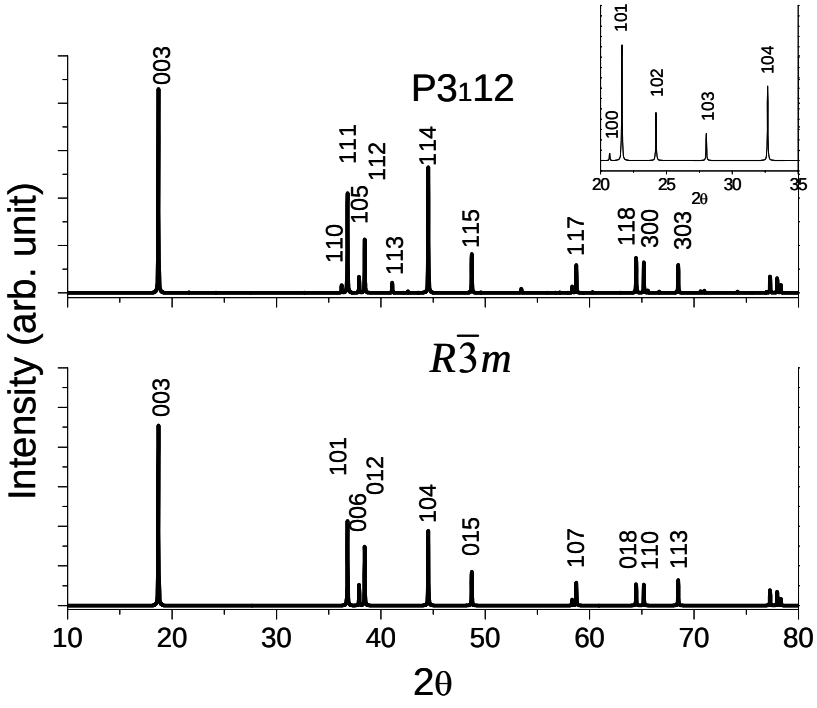

Fig. 2.8: X-ray diffraction spectra of $LiNi_{1/3}Mn_{1/3}Co_{1/3}O_2$ with $R\bar{3}m$ and $P3_112$ space group simulated using program Powdercell. The superreflections of $P3_112$ between 20˚ and 35˚ were enlarged.

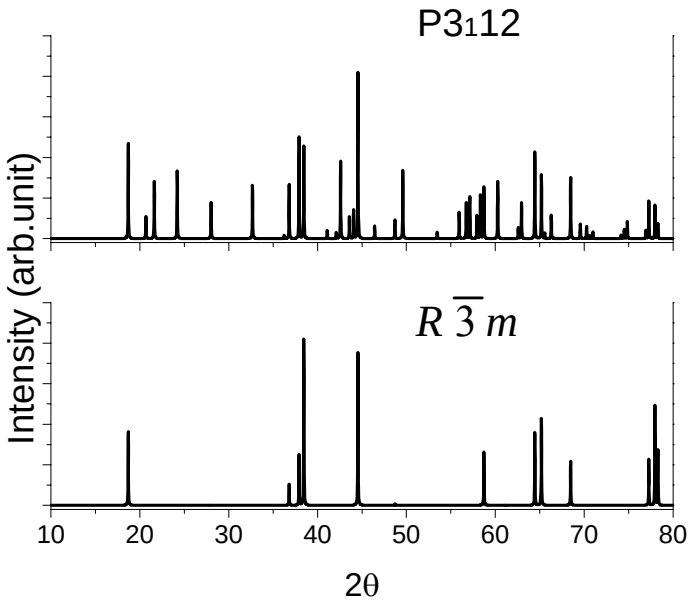

Fig. 2.9: Neutron diffraction spectra of $LiNi_{1/3}Mn_{1/3}Co_{1/3}O_2$ with $R\bar{3}m$ and $P3_112$ space group simulated using program Powdercell.

2.6 Conclusions

Both virgin and cycled (discharged status) $LiNi_{1/3}Mn_{1/3}Co_{1/3}O_2$ specimens were investigated by transmission electron microscopy. This $LiNi_{1/3}Mn_{1/3}Co_{1/3}O_2$ material was found to be inhomogeneous according to our study. 15 randomly selected particles of pristine $LiNi_{1/3}Mn_{1/3}Co_{1/3}O_2$ were analyzed, in which 10 particles (66.7%) were single crystals, 5 particles (33.3%) were polycrystalline crystals. They contain 6 particles (40%) with superstructures. The inhomogeneous phenomenon was also found in cycled samples from corn cells. Only 2 (10%) particles out of 20 randomly selected particles of $LiNi_{1/3}Mn_{1/3}Co_{1/3}O_2$ sample at discharged status after charged to 5.2 V contain superstructures. Obviously, the number of superstructures of cycled sample (10%) was much smaller than pristine $LiNi_{1/3}Mn_{1/3}Co_{1/3}O_2$

sample (40%). $R\bar{3}m$ symmetry was the majority structure for $LiNi_{1/3}Mn_{1/3}Co_{1/3}O_2$. Superstructure was very common in $LiNi_{1/3}Mn_{1/3}Co_{1/3}O_2$ due to the arrangements of three transition metallic ions Ni, Mn, and Co and the disorder of Li/Ni. Among those superstructures, $P3_112$ symmetry was the main superlattice of this material with a particular arrangement of TM ions in TM layers called $[\sqrt{3}\times\sqrt{3}]R30^0$-type structure. $P3_112$ superstructure was hardly distinguished by XRD experimentally since $P3_112$ and $R\bar{3}m$ structures had similar X-ray diffraction spectra. While they had distinct neutron spectra indicating neutron diffraction is a good experimental method to identify $P3_112$ superstructure from $R\bar{3}m$ phase.

2.7 References

(1) Mizushima, K.; Jones, P. C.; Wiseman, P. J.; Goodenough, J. B. *Materials Research Bulletin* **1980**, *15*, 783-789.
(2) Ohzuku, T.; Makimura, Y. *Chem. Lett.* **2001**, 30, 744.
(3) Makimura, Y.; Ohzuku, T. *J. Power sources* **2003**, 119, 156.
(4) Lu, Z. H.; Beaulieu, L. Y.; Donaberger, R. A.; Thomas, C. L.; Dahn, J. R. *J Electrochem Soc* **2002**, *149*, A778.
(5) Lu, Z. H.; MacNeil, D. D.; Dahn, J. R. *Electrochemical and Solid-State Letters* **2001**, *4*, A191.
(6) Kang, K.; Meng, Y. S.; Breger, J.; Grey, C. P.; Ceder, G. *Science* **2006**, *311*, 977-980.
(7) Lu, Z. H.; Chen, Z. H.; Dahn, J. R. *Chem. Mater.* **2003**, *15*, 3214.
(8) Meng, Y. S.; Ceder, G.; Grey, C. P.; Yoon, W. S.; Shao-Horn, Y. *Electrochemical and Solid-State Letters* **2004**, *7*, A155-A158.
(9) Meng, Y. S.; Ceder, G.; Grey, C. P.; Yoon, W. S.; Jiang, M.; Breger, J.; Shao-Horn, Y. *Chem. Mater.* **2005**, *17*, 2386-2394.
(10) Li, H. H.; Yabuuchi, N.; Meng, Y. S.; Kumar, S.; Berger, J.; Grey, C. P.; Shao-Horn, Y. *Chem. Mater.* **2007**, *19*, 2551-2565.
(11) Hinuma, Y.; Meng, Y. S.; Kang, K.; Ceder, G. *Chem. Mater.* **2007**, *19*, 1790-1800.
(12) Breger, J.; Meng, Y. S.; Hinuma, Y.; Kumar, S.; Kang, K.; Shao-Horn, Y.; Ceder, G.; Grey, C. P. *Chem. Mater.* **2006**, *18*, 4768-4781.
(13) Ohzuku, T.; Makimura, Y. *Chem. Lett.* **2001**, *30*, 642.
(14) Kim, H.-S.; Kim, S.-I.; Kim, W.-S. *Electrochimica Acta* **2006**, *52*, 1457-1461.
(15) Choi, J.; Manthiram, A. *J Electrochem Soc* **2005**, *152*, A1714-A1718.
(16) Amatucci, G. G.; Tarascon, J. M.; Klein, L. C. *J. electrochem. soc.* **1996**, *143*, 1114-1123.
(17) Ceder, G.; Ven, A. V. d.; Aydinol, M. K. *J. of metal, materials and mimerals* **1998**.
(18) Li, D.; Muta, T.; Zhang, L.; Yoshio, M.; Noguchi, H. *J. Power sources* **2004**, *132*, 150-155.
(19) Yabuuchi, N.; Ohzuku, T. *J. Power sources* **2003**, *119-121*, 171-174.

(20) Koyama, Y.; Makimura, Y.; Tanaka, I.; Adachi, H.; Ohzuku, T. *J Electrochem Soc* **2004**, *151*, A1499-1506.
(21) Koyama, Y.; Yabuuchi, N.; Tanaka, I.; Adachi, H.; Ohzuku, T. *J. Electrochem. Soc* **2004**, *151*, A1545-A1551.
(22) Koyama, Y.; Tanaka, I.; Adachi, H.; Ohzuku, T. *J. Power sources* **2003**, *119-121*, 644-648.
(23) Yoon, W.-S.; Grey, C. P.; Balasubramanian, M.; Yang, X.-Q.; Fischer, D. A.; McBreen, J. *Electrochemical and Solid-State Letters* **2004**, *7*, A53-A55.
(24) Nedoseykina, T.; Kim, S.-S.; Nitta, Y. *elelctrochim ACTA* **2006**, *52*, 1467-1471.
(25) Li, D.-C.; Muta, T.; Zhang, L.-Q.; Yoshio, M.; Noguchi, H. *J. Power sources* **2004**, *132*, 150-155.
(26) He, P.; Wang, H.; Qi, L.; Osaka, T. *J. Power sources* **2006**, *160*, 627-632.
(27) Kim, H.-s.; Lee, C.; Moon, S. *J. Power sources* **2006**, *159*, 227-232.
(28) Luo, X.; Wang, X.; Liao, L.; Wang, X.; Gamboa, S.; Sebastian, T. J. *J. Power sources* **2006**, *161*, 601-605.
(29) Yabuuchi, N.; Makimura, Y.; Ohzuku, T. *J Electrochem Soc* **2007**, *154*, A314-321.
(30) Chen, Z.; Sun, Y. K.; Amine, K. *J Electrochem Soc* **2006**, *153*, A1818-1822.
(31) Kim, J.-M.; Kumagai, N.; Komaba, S. *elelctrochim ACTA* **2006**, *52*, 1483-1490.
(32) Kobayashi, H.; Arachi, Y.; Emura, S.; Kageyama, H.; Tatsumi, K.; Kamiyama, T. *J. Power sources* **2005**, *146*, 640-644.
(33) Li, D.; Sasaki, Y.; Kobayakawa, K.; Noguchi, H.; Sato, Y. *elelctrochim ACTA* **2006**, *52*, 643-648.
(34) Kobayakawa, M.; Li, D.; Kobayakawa, K.; Sato, Y.; Lee, Y. S. *J. Power sources* **2006**, *157*, 494-500.
(35) Li, D.; Kato, Y.; Kobayakawa, K.; Noguchi, H.; Sato, Y. *J. Power sources* **2006**, *160*, 1342-1348.
(36) Kim, H.-S.; Kim, S.-I.; Kim, W.-S. *elelctrochim ACTA* **2006**, *52*, 1457-1461.
(37) Whitfield, P. S.; Davidson, I. J.; Cranswick, L. M. D.; Swainson, I. P.; Stephens, P. W. *Solid State Ionics* **2005**, *176*, 463-471.
(38) Ven, A. V. d.; Ceder, G. *Electrochemistry Communications* **2004**, *6*, 1045-1050.

Appendix

Appendix A: unit cell of pile-up model.

Element	x	y	z
Li	2/3	0	1/6
Li	1/3	2/3	1/2
Li	2/3	2/3	5/6
Li	0	0	1/2
Li	0	2/3	1/6
Li	0	1/3	1/6
Li	2/3	1/3	5/6
Li	1/3	1/3	1/2
Ni	1/3	1/3	2/3
Co	0	0	0
Mn	1/3	0	1/3
Mn	2/3	2/3	1/3
Ni	2/3	0	2/3
Co	1/3	2/3	0
Ni	0	2/3	2/3
Co	2/3	1/3	0
Mn	0	1/3	1/3
O	1/3	0	7/12
O	0	2/3	11/12
O	2/3	1/3	1/4
O	2/3	0	11/12
O	0	1/3	7/12
O	1/3	2/3	1/4
O	2/3	2/3	7/12
O	1/3	1/3	11/12
O	0	0	1/4
O	0	0	3/4
O	1/3	1/3	5/12
O	2/3	2/3	1/12
O	2/3	1/3	3/4
O	1/3	0	1/12
O	0	2/3	5/12
O	1/3	2/3	3/4
O	2/3	0	5/12
O	0	1/3	1/12

Appendix B: unit cell of $[\sqrt{3}\times\sqrt{3}]R30^0$ model with partial Li/Ni interchange.

Element	Wyckoff	x	y	z
Li(1)	3b	0.7785	0.8892	0.5
Ni	3b	0.7785	0.8892	0.5
Li(2)	3b	0.1178	0.5589	0.5
Ni	3b	0.1178	0.5589	0.5
Li(3)	3b	0.4348	0.2174	0.5
Ni	3b	0.4348	0.2174	0.5
Co	3a	0.7773	0.8886	0
Ni	3a	0.1106	0.5553	0
Li	3a	0.1106	0.5553	0
Mn	3a	0.4457	0.2228	0
O(1)	6c	0.7950	0.9020	0.2564
O(2)	6c	0.0977	0.5589	0.2553
O(3)	6c	0.4402	0.2046	0.2558

Appendix C: unit cell of O3 model with partial Li/Ni interchange.

Element	Wyckoff	x	y	z
Ni	3a	0	0	0
Li	3a	2/3	1/3	1/3
Li	3a	1/3	2/3	2/3
Co/Ni/Mn	3b	0	0	0.5
Co/Ni/Mn	3b	2/3	1/3	5/6
Co/Ni/Mn	3b	1/3	2/3	1/6
O	6c	0	0	0.23950
O		0	0	0.76050
O		2/3	1/3	0.57283
O		2/3	1/3	0.09383
O		1/3	2/3	0.90617
O		1/3	2/3	0.42717

VITA

Tanghong Yi was born in Yichang, China in February 1983. He obtained his B.S. of Material Science and Engineering in the University of Science and Technology of China in 2005. In the same year of the graduation, he came to the University of New Orleans and joined Dr. Heike Gabrisch's group in Department of Chemistry/Advanced Materials Research Institute.